Experimental Validation of a Finite Element Model of a Flexible Parallel Manipulator

Fernanda T. Colombo[1], Maíra M. da Silva[1]

[1]*Department of Mechanical Engineering, São Carlos School of Engineering, University of São Paulo*
Trabalhador São-Carlense, 400, 13566-590, São Carlos/SP, Brazil
fernanda.colombo@usp.br, mairams@sc.usp.br

Abstract. Parallel manipulators present better dynamic performance than serial robots in terms of positioning accuracy and operating speeds. However, it is complex to develop control strategies for parallel robots due to the difficulty of obtaining the end-effector's pose given the position of the joints. This task can be even more complicated if the robot is lightweight and the links are flexible. A model of the system's dynamics can be used in the design of model-based controllers and may be essential to improve the performance of flexible manipulators subject to undesired vibration. In this paper, we developed in a multibody dynamics environment a finite element model of the parallel manipulator 3RRR. The current setup has thin and light links connecting the revolute joints of each one of the three kinematic chains. To validate the multibody model implemented, we performed an experimental modal test with accelerometers placed on the links and a roving impact hammer. Modal parameters such as the natural frequencies of the numerical model and experimental setup were compared for different poses of the manipulator.

Keywords: Multibody Dynamics, Experimental Modal Analysis

1 Introduction

The demand for cost-efficiency design processes enforces minimal prototyping, relying on numerical simulation for evaluating the design requirements. Moreover, reliable, accurate, and time-efficient numerical models can be used for control design, predicting maintenance, estimating states, and assessing uncertainties. The design of a mechatronic system is a complex and multidisciplinary task since it merges different fields such as mechanics, electronics, control, piezoelectricity, among others [1]. Therefore, the numerical tools must allow the designer to work with diverse subsystems, enabling integration throughout the design process and providing decision-making tools.

Despite this necessity, there is a gap between the software used to evaluate mechanical structures to design control strategies. On the one hand, mechanical engineers employ finite-element and multibody packages to assess the system dynamics. On the other hand, control engineers use input-output dynamic modeling representation. Therefore, the designer should reduce CAD-based models to low-order ones that can be used in control design schemes. A Global Modal Parametrization has been proposed by [2] aiming the extraction of compact ordinary differential equations (ODEs) in closed-form. This methodology has been exploited by [3] for deriving suitable models of a flexible parallel manipulator.

Flexible manipulators can be more energy-efficient and may offer higher dynamic performance. However, these manipulators are complex systems, and their design presents the same issues related to the design of any mechatronic system. In addition, the designer should consider the links' deformation of this kind of manipulator when evaluating its performance or designing its control [4]. Figure 1 illustrates a typical control scheme for a flexible manipulator. Usually, a large amount of data has to be acquired, evaluated, and treated. This data can be fed back to the control law. The control law scheme may use terms from the kinematic and dynamic models.

The complexity of controlling a parallel manipulator is notably higher due to the lack of a direct measurement of the pose (position and orientation) of the manipulator's end-effector [5]. This complexity may be more critical if the manipulators under study are subject to vibrations due to the flexibility of their components. One alternative

for designing Cartesian control strategies, which require the measurement of the end-effector pose, is the use of vision-based techniques and image processing algorithms [6, 7].

The present manuscript aims to contribute to the field of flexible manipulators by modeling a parallel manipulator with flexible links. This task is of utmost importance for the control of such a machine. Moreover, challenges as the configuration-dependent dynamics and the modeling procedure are discussed. The finite element model is validated with experimental data. And, a reduced model is derived for control purposes.

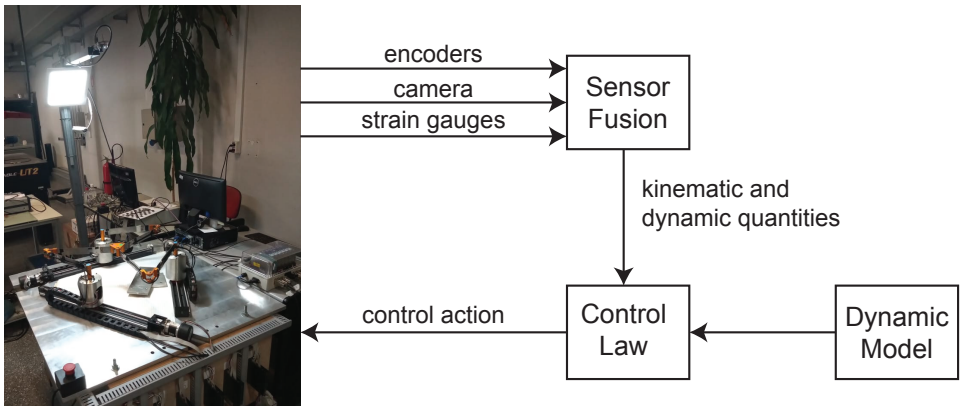

Figure 1. Control scheme for a flexible manipulator

2 Finite Element Model

In structural mechanics problems, the displacements and deformations of a structure due to force loads and support conditions are investigated. In most cases, exact solutions for these boundary value problems are not available. The Finite Element (FE) method provides an approximate solution by substituting the original complex problem, usually a partial differential equation, by a system of ordinary differential equations. After dividing the structure's geometry into several smaller pieces, called elements, the mass and stiffness of each element are derived by physical principles, such as equilibrium conditions and variational principles. Considering that the displacement field within each element is piecewise continuous, the displacement of the nodes located in the boundary of the elements is not known but can be approximated by polynomial functions. The FE model can be described by

$$\begin{aligned} \mathbf{M}\,\ddot{\mathbf{q}} + \mathbf{K}\,\mathbf{q} &= \mathbf{b}_f\,\mathbf{u}, \\ \mathbf{y} &= \mathbf{c}_y\,\ddot{\mathbf{q}}, \end{aligned} \tag{1}$$

where $\mathbf{M} \in \mathbb{R}^{n\times n}$ and $\mathbf{K} \in \mathbb{R}^{n\times n}$ are the mass and stiffness matrices, respectively, and n is the number of degrees of freedom in the FE model, described by the nodal displacement vector $\mathbf{q} \in \mathbb{R}^n$. The input vector $\mathbf{u} \in \mathbb{R}^{n_u}$ represents the forces applied in the n_u actuated nodes defined in the Boolean matrix $\mathbf{b}_f \in \mathbb{R}^{n\times n_u}$. The output vector $\mathbf{y} \in \mathbb{R}^{n_y}$ denotes the acceleration of the n_y measured nodes described by the Boolean matrix $\mathbf{c}_y \in \mathbb{R}^{n_y\times n}$. The boundary conditions of the problem are assumed to have already been incorporated into this model.

To solve this system of ordinary differential equations and obtain the nodal displacement vector, we can first rewrite this problem in modal coordinates instead of directly integrating it. Transforming the displacement vector by $\mathbf{q} = \boldsymbol{\Phi}\,\boldsymbol{\eta}$, we can rewrite eq. (1) as

$$\begin{aligned} \boldsymbol{\Phi}^T\,\mathbf{M}\,\boldsymbol{\Phi}\,\ddot{\boldsymbol{\eta}} + \boldsymbol{\Phi}^T\,\mathbf{K}\,\boldsymbol{\Phi}\,\boldsymbol{\eta} &= \boldsymbol{\Phi}^T\,\mathbf{b}_f\,\mathbf{u}, \\ \mathbf{y} &= \mathbf{c}_y\,\boldsymbol{\Phi}\,\ddot{\boldsymbol{\eta}}, \end{aligned} \tag{2}$$

where $\boldsymbol{\Phi} \in \mathbb{R}^{n\times r}$ is the modal matrix and $\boldsymbol{\eta} \in \mathbb{R}^r$ is the modal coordinates vector. The modal matrix contains only the first r mode shapes of the structure, as $\boldsymbol{\Phi} = \begin{bmatrix}\phi_1 & \phi_2 & \dots & \phi_r\end{bmatrix}$, obtained by solving the eigenvalue problem $(\mathbf{K} - \omega^2\mathbf{M})\boldsymbol{\Phi} = \mathbf{0}$. With $r \ll n$, this transformation significantly reduces the order of the problem [8]. Also, the

orthogonality conditions between the mode shapes imply that $\mathbf{\Phi}^T\ \mathbf{M}\ \mathbf{\Phi} = \text{diag}(\mu_i)$ and $\mathbf{\Phi}^T\ \mathbf{K}\ \mathbf{\Phi} = \text{diag}(\mu_i\ \omega_i^2)$, where μ is the modal mass and ω is the natural frequency. Classical damping can be added to the model as a diagonal matrix $\bar{\mathbf{D}}$ proportional to the velocity term and defined by $\bar{\mathbf{D}} = \text{diag}(2\ \xi_i\ \mu_i\ \omega_i)$, where ξ is the modal fraction of critical damping. Considering zero initial conditions, the FE model can be rewritten in modal coordinates as

$$\begin{aligned} \ddot{\boldsymbol{\eta}} + 2\,\boldsymbol{\xi}\,\boldsymbol{\Omega}\,\dot{\boldsymbol{\eta}} + \boldsymbol{\Omega}^2\,\boldsymbol{\eta} &= \boldsymbol{\mu}^{-1}\,\mathbf{\Phi}^T\,\mathbf{b}_f\,\mathbf{u}, \\ \mathbf{y} = \mathbf{c}_y\,\mathbf{\Phi}\,(-\boldsymbol{\Omega}^2\,\boldsymbol{\eta} - 2\,\boldsymbol{\xi}\,\boldsymbol{\Omega}\,\dot{\boldsymbol{\eta}} + \boldsymbol{\mu}^{-1}\,\mathbf{\Phi}^T\,\mathbf{b}_f\,\mathbf{u}), \end{aligned} \tag{3}$$

where $\boldsymbol{\mu} = \text{diag}(\mu_i)$, $\boldsymbol{\Omega} = \text{diag}(\omega_i)$ and $\boldsymbol{\xi} = \text{diag}(\xi_i)$, or in the state-space form:

$$\begin{aligned} \begin{bmatrix} \dot{\boldsymbol{\eta}} \\ \ddot{\boldsymbol{\eta}} \end{bmatrix} &= \begin{bmatrix} \mathbf{0} & \mathbf{I} \\ -\boldsymbol{\Omega}^2 & -2\,\boldsymbol{\xi}\,\boldsymbol{\Omega} \end{bmatrix} \begin{bmatrix} \boldsymbol{\eta} \\ \dot{\boldsymbol{\eta}} \end{bmatrix} + \begin{bmatrix} \mathbf{0} \\ \boldsymbol{\mu}^{-1}\,\mathbf{\Phi}^T\,\mathbf{b}_f \end{bmatrix} \mathbf{u}, \\ \mathbf{y} = \mathbf{c}_y\,\mathbf{\Phi} \begin{bmatrix} -\boldsymbol{\Omega}^2 & -2\,\boldsymbol{\xi}\,\boldsymbol{\Omega} \end{bmatrix} &\begin{bmatrix} \boldsymbol{\eta} \\ \dot{\boldsymbol{\eta}} \end{bmatrix} + \begin{bmatrix} \mathbf{c}_y\,\mathbf{\Phi}\,\boldsymbol{\mu}^{-1}\,\mathbf{\Phi}^T\,\mathbf{b}_f \end{bmatrix} \mathbf{u}. \end{aligned} \tag{4}$$

3 Parallel Manipulator

The robotic manipulator studied in this project is the parallel manipulator 3RRR, illustrated in Fig. 2, which has three revolute joints (RRR) in each of the three (3) kinematic chains. Only the first revolute joints of each chain are active as their motion are driven by an external torque. The pose of its end-effector $\mathbf{X} = [x, y, \alpha]^T$, described by the displacement in the x and y directions and the angular position α, is used to define the manipulator's configuration. In the manipulator's prototype, seen in Fig. 2(b), three brushless Maxon EC60 flat motors with Maxon EPOS2 50/5 controllers are used in the active joints [9]. The stress and acceleration of some points of the links are measured by strain gauges and accelerometers placed on them. Moreover, the end-effector's pose is estimated in real-time by a computer vision algorithm [7].

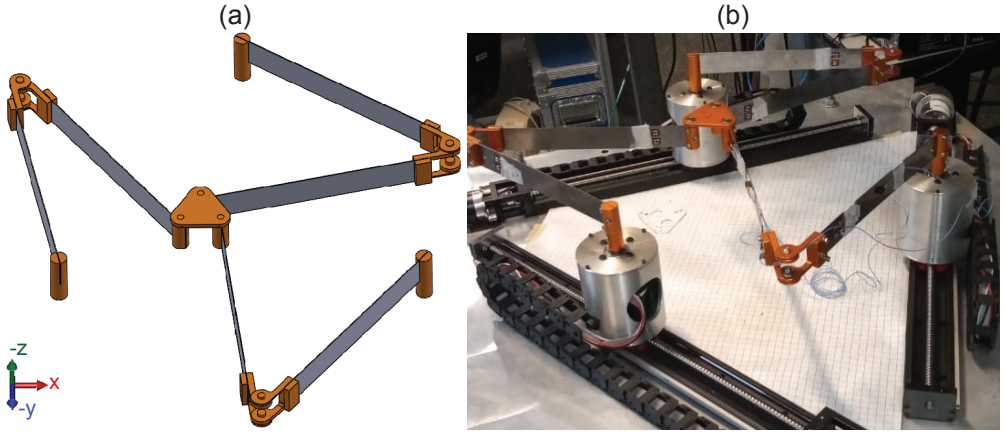

Figure 2. 3RRR parallel manipulator: CAD model (a) and prototype (b)

The components were designed and assembled using the computer-aided design (CAD) software SolidWorks 2018. Based on this CAD assembly, a numerical model of the parallel manipulator 3RRR was implemented using the FE method in the Multibody Dynamics (MBD) environment of the Comsol Multiphysics 5.5 software. The revolute joints were modeled using the hinge joint available in this MBD package, which constrains the motion of two components to rotate along the joint axis.

To reduce the number of degrees of freedom in this model, we assumed that only the links and end-effector are flexible without causing a significant decrease in the model's accuracy. Moreover, we considered that the

components have a linear elastic behavior and can be modeled as an isotropic solid. The material of the end-effector and joints is aluminum, and their material properties are listed in Table 1. The properties of the links had to be experimentally estimated to include the mass of the strain gauges, accelerometers, and cables. All the sensors placed on the links were responsible for a considerable increase in the links' weight since these steel SAE 1040 links are thin (0.70 mm $\times$ 35 mm $\times$ 300 mm) and very light (0.06 kg). Since most cables and sensors are located in the links closer to the motors, the final weight of the first links of each kinematic chain is greater than the weight of the second links, which are closer to the end-effector. The mesh created has tetrahedral elements with a displacement field approximated by a quadratic function and $n = 13989$ degrees of freedom.

Table 1. Material properties of the 3RRR manipulator's components

Components	Density (kg/m^3)	Poisson's ratio	Young's modulus (GPa)
First links	12500	0.3	200
Second links	9500	0.3	220
End-effector and joints	2800	0.33	70

In the Comsol environment, we performed an eigenfrequency study to analyze the manipulator's mode shapes, frequency bandwidth, and the most appropriate sensor and excitation locations. The displacement of the active joints was constrained in this test to simulate a stationary configuration of the manipulator. For the end-effector's pose $\mathbf{X}$ = [-5 cm, -5 cm, 0°]^T, Fig. 3 illustrates six modes shapes of the manipulator and the corresponding natural frequencies. The first three modal displacements are rigid body modes, which coincides with the three degrees of freedom that the manipulator presents. The remaining mode shapes correspond to the (out-of-plane) bending of the flexible links. Due to the similarities between all the links, modes 1-3, and 4-6 are closely spaced in frequency, as they present almost repeated natural frequencies. Also, not every component of this structure can be excited by these modes. An experimental modal test should be carried out to validate this FE model taking these difficulties into account. Finally, we exported the matrices $\mathbf{M}$ and $\mathbf{K}$ and vectors $\mathbf{b}_f$ and $\mathbf{c}_y$ to Matlab 2015a, together with additional information about the coordinates and constraints of the nodes. The state-space formulation described in the last section is used to investigate further the model's frequency response.

4 Experimental Modal Analysis

Experimental data on the manipulator's prototype was used to validate the FE model developed. A modal analysis was performed to obtain the prototype's dynamic properties with three single-axis accelerometers PCB 352A24 and a roving impact hammer with a force transducer PCB 208C02. We selected the ends and middle points of each link as the sensors and excitation locations. A multiple-input multiple-output (MIMO) modal test is recommended to detect closely spaced modes. For each sensor/transducer configuration, the data from five impacts were acquired and averaged to obtain the manipulator's frequency response function (FRF) with a frequency bandwidth of 250 Hz and resolution of 0.3125 Hz. After inspecting all acquired data, we selected the configurations that provided the best responses in low frequency to form the FRF matrix $\mathbf{H}(j\omega) \in \mathbb{R}^{n_u \times n_y}$.

To estimate the modal parameters of this experimental data, we applied the complex mode indicator function (CMIF) based on the singular value decomposition of the FRF matrix [10, 11]. At each frequency ω, $\mathbf{CMIF} \in \mathbb{R}^{n_y \times n_y}$ is defined as

$$\begin{aligned} \mathbf{H}(j\omega) &= \mathbf{U}(j\omega)\, \mathbf{S}(j\omega)\, \mathbf{V}^*(j\omega), \\ \mathbf{CMIF}(j\omega) &= \mathbf{S}(j\omega)^T\, \mathbf{S}(j\omega), \end{aligned} \tag{5}$$

where the matrices $\mathbf{U} \in \mathbb{R}^{n_u \times n_u}$ and $\mathbf{V}^* \in \mathbb{R}^{n_y \times n_y}$ contain the left and right singular vectors, respectively, and $\mathbf{S} \in \mathbb{R}^{n_u \times n_y}$ is a diagonal matrix with singular values. The symbol $*$ denotes the complex conjugate matrix.

Since multiple excitation and measurement points are available, CMIF can be used to identify the natural frequencies of even closely spaced modes. Figure 4 illustrates the CMIF values obtained for the end-effector pose $\mathbf{X}$ = [-5 cm, -5 cm, 0°]^T as a function of frequency. The frequencies at the peaks of the CMIF curve with the largest singular values (in blue) represent the system's natural frequencies. However, not all peaks in this curve

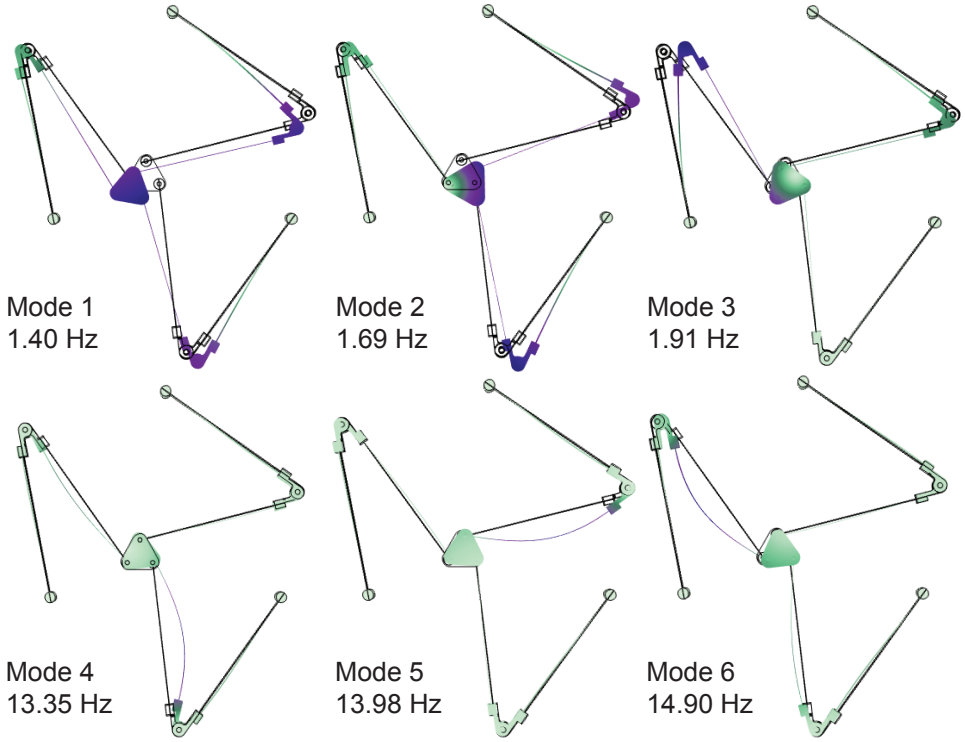

Figure 3. First six modes shapes and corresponding natural frequencies of the 3RRR manipulator's FE model, for the end-effector's pose $\mathbf{X}$ = [-5 cm, -5 cm, 0°]^T

indicate a system mode as they may be caused by noise or errors during the modal analysis and must be carefully selected. Multiple modes in the same frequency range can be detected if the remaining CMIF curves present peaks at the same frequency as the first one. In addition to the CMIF values, Figure 4 shows the selected peaks, and many peaks occur at the same frequency for all three CMIF curves as predicted by the FE model.

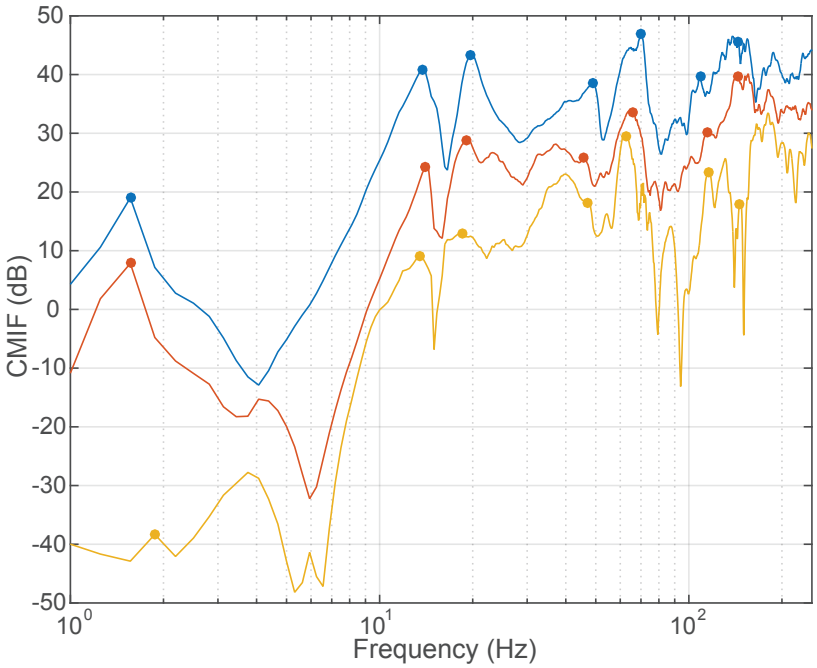

Figure 4. Experimental CMIF values in function of frequency and selected peaks indicated by circles, for the end-effector's pose $\mathbf{X}$ = [-5 cm, -5 cm, 0°]^T

5 Results and Discussion

To validate the numerical model developed, we compared the natural frequencies of the FE model with the experimental values determined by the CMIF curves. Table 2 illustrates the natural frequencies of the first ten modes of the manipulator and the relative error between the numerical and experimental values for two different manipulator's poses. Although there is a considerable relative error of 11% for some rigid-body modes, the frequency resolution used in the modal analysis was not small enough to adequately capture the manipulator's dynamics at such a low frequency. For both manipulator's poses, the modal analysis missed the tenth mode, which corresponds to the in-plane bending of the links. As only single-axis accelerometers were available, the vertical motion of this mode shape was not tracked by the experiments. Using the CMIF values in function of frequency was a successful estimation tool of the natural frequencies of this manipulator, as all closely spaced bending modes were detected in this frequency range. With an average error of 5.3% and 7.8% for poses $\mathbf{X}$ = [-5 cm, -5 cm, $0^\circ]^T$ and $\mathbf{X}$ = [+5 cm, +5 cm, $0^\circ]^T$, respectively, there is a good correlation between the numerical and experimental data in terms of natural frequency.

Table 2. Comparison between the natural frequencies of the FE model and the experimental modal analysis (EMA) for two manipulator's poses

	$\mathbf{X}$ = [-5 cm, -5 cm, $0^\circ]^T$			$\mathbf{X}$ = [+5 cm, +5 cm, $0^\circ]^T$		
Mode	FE (Hz)	EMA (Hz)	Relative Error	FE (Hz)	EMA (Hz)	Relative Error
1	1.40	1.56	11.43%	1.39	1.36	2.16%
2	1.69	1.56	7.69%	1.77	1.56	11.86%
3	1.91	1.87	2.09%	1.83	1.67	8.74%
4	13.35	13.44	0.67%	13.52	13.44	0.59%
5	13.98	13.75	1.65%	13.82	14.38	4.05%
6	14.90	14.06	5.64%	14.76	15.00	1.63%
7	20.13	18.44	8.40%	19.49	16.25	16.62%
8	20.25	19.06	5.88%	19.66	16.88	14.14%
9	20.61	19.69	4.46%	20.03	17.81	11.08%
10	45.66	-	-	46.16	-	-

Considering a force input at the middle of the first link and the acceleration of the end of the second link as output, Fig. 5 illustrates the frequency response of this system obtained by the modal analysis. The experimental FRF confirms that the manipulator's mode shapes are not well separated and present relatively heavy damping. Damped responses are typical in robotic manipulators due to the friction between the joints' components. Nonetheless, estimating the modal parameters of such a system is a difficult task. Moreover, Fig. 5 shows the numerical FRF obtained by the FE model in the state-space form, with $r = 350$ modes. Both responses have a good agreement, especially below 30 Hz, which includes the first nine mode shapes. Measurement noise and the difficulty in defining the correct location and direction that the force is applied or the acceleration is measured in the FE model may also contribute to the discrepancies seen in this graph.

6 Conclusions

In a multibody dynamics software based on the finite element method, we obtained a numerical model of the 3RRR manipulator, a lightweight parallel manipulator with flexible links. Since this dynamic model may be essential to improve the performance of the prototype subject to unwanted vibration, we evaluated the validity of this modeling technique by comparing the frequency responses of the model and the experimental modal analysis. With closely spaced and highly damped modes, the complex mode indicator function was used to estimate the system's natural frequencies from the experimental data. The numerical model provided a good approximation of the prototype's dynamics regarding frequency response and natural frequency, which presented an average relative error lower than 8% for different manipulator configurations. The validated dynamic model can be used in the control design after applying a suitable model order reduction method.

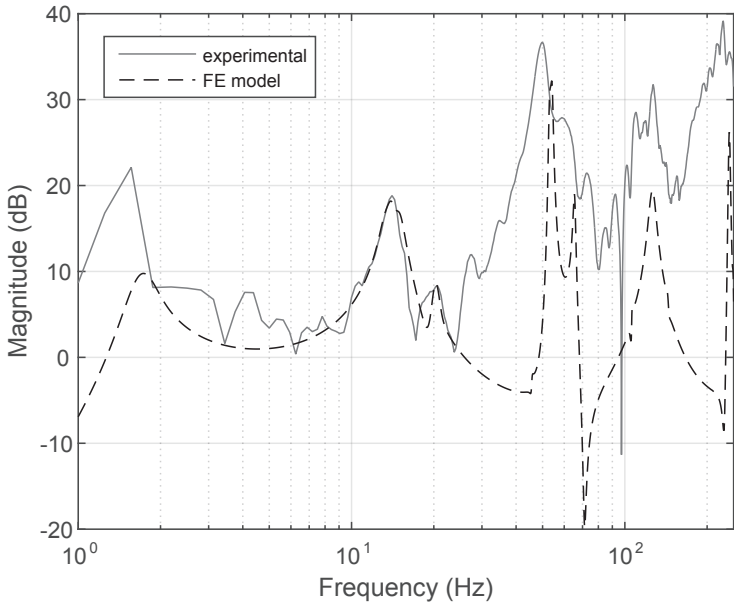

Figure 5. Comparison between the FE and experimental FRFs, considering a force input at the middle of the first link and the acceleration of the end of the second link as output, for the end-effector's pose $\mathbf{X}$ = [-5cm, -5cm, $0°]^T$

Acknowledgements. This research is supported by FAPESP 2018/21336-0. Fernanda T. Colombo and Maíra M. da Silva are thankful for their scholarships FAPESP 2018/22760-0 and CNPq 301338/2018-3, respectively.

Authorship statement. The authors hereby confirm that they are the sole liable persons responsible for the authorship of this work, and that all material that has been herein included as part of the present paper is either the property (and authorship) of the authors, or has the permission of the owners to be included here.

References

[1] da M. M. Silva and L. A. M. Gonçalves. Mechatronic design concept and its application to pick-and-place robotic systems. *Journal of the Brazilian Society of Mechanical Sciences and Engineering*, vol. 35, n. 1, pp. 31–40, 2013.

[2] O. Brüls, P. Duysinx, and J.-C. Golinval. The global modal parameterization for non-linear model-order reduction in flexible multibody dynamics. *International Journal for Numerical Methods in Engineering*, vol. 69, n. 5, pp. 948–977, 2007.

[3] da M. M. Silva, O. Brüls, J. Swevers, W. Desmet, and H. V. Brussel. Computer-aided integrated design for machines with varying dynamics. *Mechanism and Machine Theory*, vol. 44, n. 9, pp. 1733–1745, 2009.

[4] Y. Gao, F.-Y. Wang, and Z.-Q. Xiao. Mechatronic design of flexible manipulators. In *Flexible Manipulators*, pp. 185–249. Elsevier, 2012.

[5] F. Paccot, P. Lemoine, N. Andreff, D. Chablat, and P. Martinet. A vision-based computed torque control for parallel kinematic machines. In *Robotics and Automation, 2008. ICRA 2008. IEEE International Conference on*, pp. 1556–1561. IEEE, 2008.

[6] R. Garrido and A. Soria. Visual control of planar parallel robots without using velocity measurements. *Journal of Intelligent & Robotic Systems*, vol. 66, n. 1, pp. 111–124, 2012.

[7] F. T. Colombo, de J. V. Carvalho Fontes, and da M. M. Silva. A visual servoing strategy under limited frame rates for planar parallel kinematic machines. *Journal of Intelligent & Robotic Systems*, vol. 96, 2019.

[8] M. R. Hatch. *Vibration simulation using MATLAB and ANSYS*. CRC Press, 2000.

[9] de J. V. Carvalho Fontes, J. C. Santos, and da M. M. Silva. Numerical and experimental evaluation of the dynamic performance of kinematically redundant parallel manipulators. *Journal of the Brazilian Society of Mechanical Sciences and Engineering*, vol. 40, n. 3, 2018.

[10] D. J. Ewins. *Modal Testing: Theory, Practice and Application*. Research Studies Press, 2 edition, 2000.

[11] J. Zwolski. Cmif - complex mode indicator function. `https://www.mathworks.com/matlabcentral/fileexchange/9476-cmif-complex-mode-indicator-function`. MATLAB Central File Exchange, 2021.